Tradeoffs in micro-opto-electro-mechanical system materials

Cleopatra Cabuz
Honeywell Technology Center
12001 State Highway 55
Plymouth, Minnesota 55441
E-mail: ccabuz@htc.honeywell.com

Abstract. To build three-dimensional micro-opto-electro-mechanical systems (MOEMS), new materials have to be designed. However, increased manufacturability results generally in modified/degraded optical, mechanical, and electrical characteristics. The paper presents a detailed analysis of $p+$ silicon as an opto-electro-mechanical material for microresonators, and gives some hints on the problems associated with the use of low-temperature dielectric in electrostatic microactuators. All the relevant parameters of $p+$ silicon are experimentally determined and process recommendations allowing improved quality are formulated. Charge injection and trapping in low-temperature dielectric are analyzed and their impact on the behavior of the electrostatic actuators evaluated.
© *1997 Society of Photo-Optical Instrumentation Engineers* [S0091-3286(97)01505-5]

Subject terms: micro-opto-electro-mechanical systems; materials; resonators; electrostatic actuators; $p+$ silicon; dielectric.

Paper MEM-15 received Nov. 11, 1996; revised manuscript received Feb. 2, 1997; accepted for publication Feb. 6, 1997.

1 Introduction

Converting a new technical concept into a real device supposes the design and fabrication of new materials and shapes.

Electronic and optical devices are based on simple shapes and sophisticated materials. To obtain and preserve material properties, electro-optical devices are fabricated and operated in a tightly controlled environment. On the other side, micro-mechanical structures require complicated three-dimensional shapes and are more tolerant, presumably, to the atomic scale detail. In addition, in many cases, such devices must work in a harsh environment.

One of the challenges of micro-opto-electro-mechanical systems (MOEMS) is to design materials that allow both three-dimensional manufacturability and opto-electro-mechanical functionality. Can these two requirements be traded?

Resonators and electrostatic actuators are the most demanding microstructures in terms of material needs. Resonators require very well controlled mechanical parameters (stress, internal losses, Young's modulus) and, for optically addressed resonators,[1] suitable optical properties. Electrostatic actuators, especially those used in touch mode actuators,[2,3] are dominated by the electrical properties of dielectrics. To design and characterize such materials, a variety of methods have to be used. This paper will review some contributions to the understanding and characterization of MOEM materials.

Microphysical investigations [secondary ion mass spectroscopy (SIMS), microprobe Raman spectroscopy (MRS), infrared spectrometry], calibrated microscopy, resonance methods, and finite element modeling (FEM) were used for the evaluation of micromechanical resonators, while the high-frequency capacitance-voltage curves were used for the characterization of electrostatic actuators. The results show the high sensitivity of some MOEM structures to the atomic detail of their materials.

2 $p+$ Silicon Microresonators

2.1 *Characterization of Stress in $p+$ Silicon Microstructures*

2.1.1 *Generalities*

Boron doping of silicon at levels exceeding 7×10^{19} cm^{-3} ($p+$ silicon) represents an effective barrier for silicon etching in the commonly used alkaline etchants such as KOH, hydrazine, and ethylene-diamine-pyrocatechol (EDP), allowing the much-desired dimensional control of the third dimension. Various micromechanical elements can be accurately shaped in $p+$ silicon, enhancing and refining the possibilities offered by bulk micromachining.[4–11] The reduced etching rate of $p+$ layers is an intrinsic property of the material, no cooperative phenomena being involved, as in the case of electrochemical etch stop,[12,13] light-assisted etch stop,[14] or thickness monitoring.[15] Up to now, it is the most convenient etch-stop technique from a process point of view, being used in several micromachined devices, some of them commercially available.[11,16] The high level of doping required in the etch stop can be achieved by epitaxial growth, ion implantation, or diffusion. Our paper focuses on the characteristics of $p+$ layers realized by diffusion from a solid source.

The enhanced manufacturability of the $p+$ silicon is, however, associated with significant alterations in the properties of single-crystal silicon. First, the high level of doping prevents the fabrication of electronic devices inside the $p+$ microstructures. Having electronic circuits on the same wafer is, if not impossible, at least more complicated.[5] Sec-

 0091-3286/97/$10 00 © 1997 Society of Photo-Optical Instrumentation Engineers

ond, the absorption spectrum of silicon is modified, from an infrared transparent material becoming a reasonably good infrared absorber (above 60% absorption) in the 10-μm spectral region.[9,11] And finally, the mechanical properties of the low-doped single-crystal silicon are significantly altered. The extent of the damage has to be well understood and evaluated.

The different size of boron and silicon atoms, with the Pauling's covalent radius of boron atom being smaller than the radius of silicon atom (0.88 Å for boron vs. 1.17 Å for silicon) generates a high intrinsic tensile stress in the heavily doped layer. At the high temperatures of diffusion or epitaxy (over 1000 °C), at a certain concentration and related to the thickness of the doped layer, the yield level is reached and the stress is released through the plastic deformation of the lattice.[17] Dislocations are generated and the strain decreases from about 5.5×10^{-4} at the yield level (concentration $1.1\times10^{20}\ \mathrm{cm}^{-3}$, stress about 67 MPa) to about 2.5×10^{-4} in the final layer (higher concentrations, stress about 30 MPa).[17] During the subsequent process steps (oxidation, annealing at high temperatures), the $p+$ layers show a transition from the relatively high tensile stress to a relatively high compressive stress. To understand why this happens, typical solid state phenomena such as diffusion, segregation, lattice mismatch, and bulk/surface plastic deformation have to be considered.

2.1.2 *Experiment*

The experiment used to clarify the mechanical behavior of the $p+$ layers is presented in Ref. 18. Both the necessary mechanical structures and boron profiles were generated. Bridges, cantilevers, and diaphragms were used for the evaluation of the average stress and the stress gradient in the layer. Low and high thermal budget paths, one-side and two-side etching, annealing, and different etching solutions were chosen to generate different boron profiles.

To evaluate the mechanical properties of the structures, the following measurements were performed:

1. The deflection of cantilevers was measured with a focused calibrated microscope and used as an indication of the stress gradient in the $p+$ layer.
2. The measured and simulated resonance frequency of a cantilever were used for the evaluation of the Young's modulus.
3. The quality factor of cantilever type resonators was used as an indication of internal losses.
4. The temperature shift of the resonance frequency of a cantilever was measured as an indication on the temperature coefficient of the Young's modulus.
5. Raman measurements performed on cantilevers and bridges were compared to establish a relation stress/Raman shift.
6. The mechanical condition (flat or buckled) of bridges and square diaphragms obtained in different process sequences was monitored and used as an indication of the type of stress in the layer (tensile or compressive).
7. The measured and simulated resonance frequency of the bridges was used for the evaluation of the average stress in the layer; the detailed experimental setup used is presented in Refs. 19 and 20.
8. The temperature dependence of the resonance frequency of the bridges was used as an indication of the thermal expansion coefficient of $p+$ silicon.

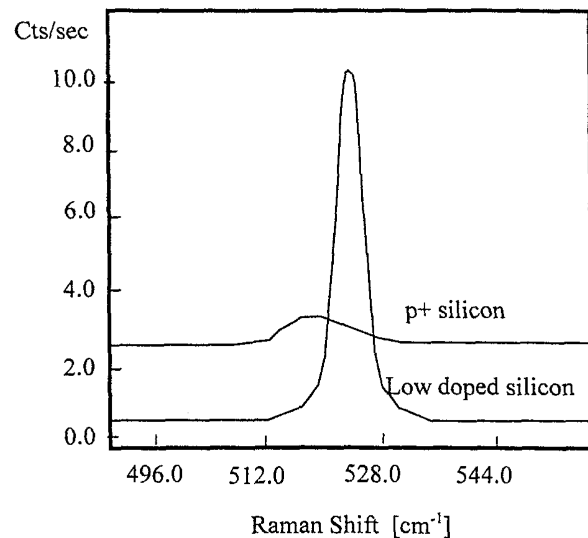

Fig. 1 Raman spectra of low-doped silicon and $p+$ silicon.

To accurately trace boron profiles in all the fabricated structures, secondary ion mass spectroscopy and microprobe Raman spectroscopy were used.[18] In the electronic devices, process simulators such as SUPREME are used for such purposes. However, $p+$ diffusion does not follow Fick's law, being not well described by such simulators. A new evaluation tool had to be developed.

2.1.3 *Results*

In Fig. 1, the one-phonon Raman spectra of silicon and $p+$ silicon are shown. The $p+$ silicon shows a shift (δ) of about $6\ \mathrm{cm}^{-1}$ toward lower frequencies compared to the low-doped silicon. The full width at half magnitude (FWHM) for low-doped silicon is about $5\ \mathrm{cm}^{-1}$ in our measurements and that for $p+$ silicon is about $22\ \mathrm{cm}^{-1}$. The intensity (I) is 7 to 8 times lower for $p+$ silicon than for low-doped silicon.

In Fig. 2 SIMS-measured boron profile (a) and features of Raman spectra as measured on as-diffused, one-side etched samples (b) are shown. The upward bending in a 2-mm-long cantilever is also represented in a schematic form in Fig. 2(c). The lower concentration in a narrow region near the diffused surface is produced by boron segregation in the thin oxide formed during diffusion (2% O_2) and cooling (50% O_2). The maximum level of boron concentration obtained in our experiment was about $1.5\times10^{20}\ \mathrm{cm}^{-3}$. The etch stop in EDP occurred at about $6\times10^{19}\ \mathrm{cm}^{-3}$. Raman shift δ and FWHM are higher for the top surface than for the back surface. These values can be related both to boron concentration and to the stress

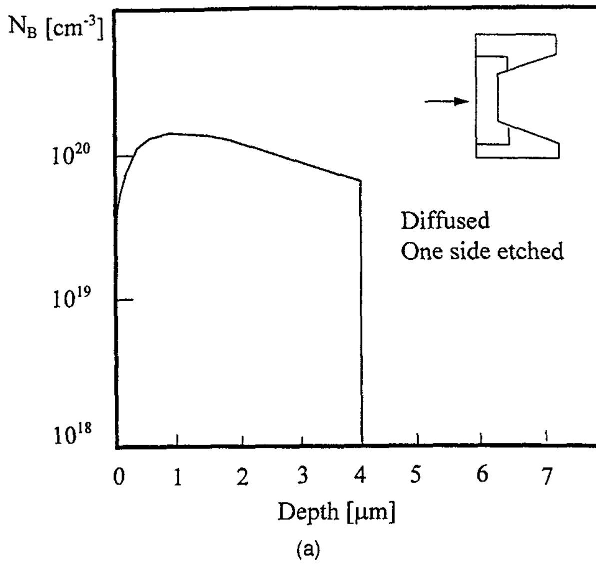

(a)

Side	δ [cm^{-1}]	FWHM [cm^{-1}]	I [cts/sec]
top	4.31	16.49	1.2
back	2.31	15.22	2

(b)

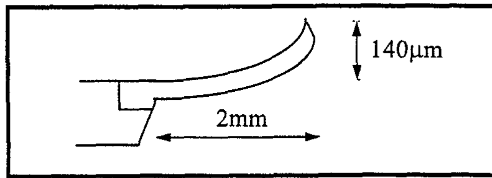

(c)

Fig. 2 SIMS-measured boron profile in as-diffused samples (a), features of Raman spectra measured on both sides of the cantilever (b), and bending of an as-diffused, one-side etched cantilever (c).

gradient. A negative stress gradient is present in the sample as we proceed from the diffused surface to the bulk, producing an upward bending of about 140 μm.

In Fig. 3 boron profile and features of Raman spectra as measured on as-diffused, both sides etched samples are shown. The SIMS profile shows that the layer with reduced boron concentration at the surface was partly etched. The upward displacement at the cantilever tip is now about 200 μm, about 4% higher than in the one-side etched sample. Raman shift δ and FWHM on the top surface are 6 cm^{-1} and 21.7 cm^{-1}, respectively, significantly higher compared to the nonetched sample.

In Fig. 4 the effect of thermal annealing on $p+$ microstructures is shown. Boron concentration became more uniformly distributed in the thickness of the layer, keeping slightly the shape of the preannealing profile. Raman measurements reflect the changes in boron profile. The cantilevers show, however, high, unexpected downward bending. This cannot be explained in the conventional way, as the cantilever bends in the direction of smaller boron concen-

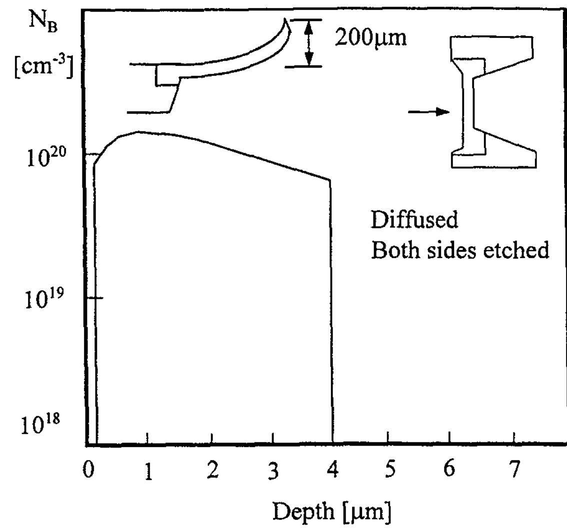

Side	δ [cm^{-1}]	FWHM [cm^{-1}]	I [cts/sec]
top	5.93	21.66	1.1
back	3.97	16.6	1.8

Fig. 3 SIMS-measured boron profile and features of Raman spectra in as-diffused, double-side etched samples.

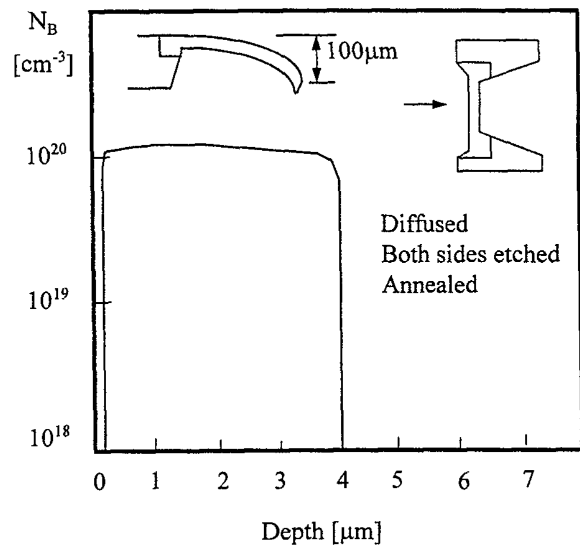

Side	δ [cm^{-1}]	FWHM [cm^{-1}]	I [cts/sec]
top	4	20.31	1.8
back	4	19.78	1.1

Fig. 4 SIMS-measured boron profile and features of Raman spectra in annealed, as-diffused, double-side etched samples.

Table 1 Mechanical evaluation of diffused/oxidized $p+$ diaphragms.

Diffusion Parameters	Oxidation Parameters	Etching Type	Shape
1160 °C, 4 h	no oxidation	one side	flat
1160 °C, 4 h	1100 °C, 20 min	one side	flat
1160 °C, 4 h	1100 °C, 80 min	one side	buckled
1160 °C, 4 h	1100 °C, 80 min	both sides	flat

tration. Since the annealing is carried out in nitrogen atmosphere, no effects related to oxide formation are responsible for this behavior. It is obvious that the thermal annealing completely changed the relation stress concentration.

Square diaphragms from $2\times2\ mm^2$ to $4\times4\ mm^2$ were fabricated and they are presented in Table 1. After oxidation, the oxide was removed from the diaphragms, so that only the $p+$ layer is responsible for the compressive stress.

2.1.4 *Discussions*

In Fig. 5 the elastic strain in a layer of boron doped silicon is shown as a function of boron concentration.[17] In the elastic region (segment a), the strain is equal to the lattice mismatch η, given by[17]

$$\eta = 1 - \frac{a'}{a_{S_i}}, \qquad (1)$$

where a' is the reduced lattice constant induced by the dopant and a_{S_i} is the lattice constant of silicon. With increasing dopant concentration, a' decreases and η, i.e., the strain, increases too.[21] The slope of segment a is given by the lattice contraction coefficient β. At a critical level, the yield strain of silicon at the diffusion temperature is

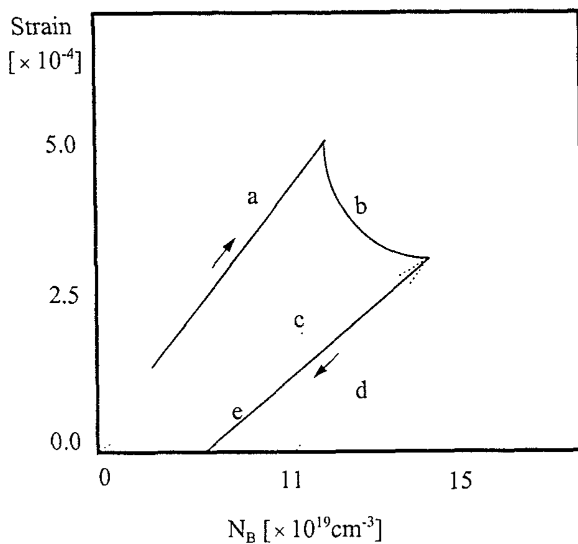

Fig. 5 Intrinsic strain vs boron concentration

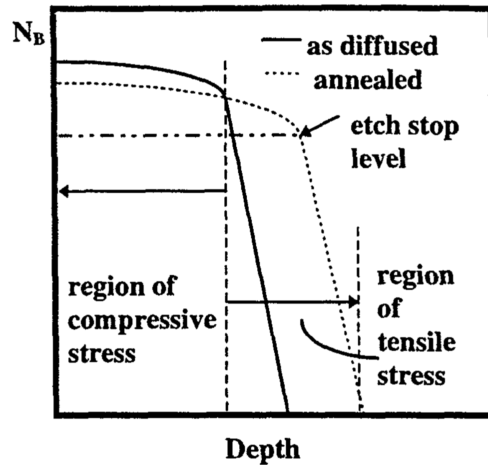

Fig. 6 Development of the compressive stress in annealed $p+$ layers.

reached and the lattice will collapse through the generation of dislocations (segment b). In this way, the overall lattice mismatch will be reduced. Plastic deformation with stress release will introduce a hysteresis in the strain-concentration characteristic. When boron out-diffuses from the layer, as actually happens in an oxidation process or a long drive-in, the residual elastic strain will relax following a curve placed inside the area limited by segments c and d in Fig. 5. In the following, we will analyze these situations.

Segment c ends in the origin of the characteristic. This means that the stress will be completely released only at zero concentration of boron. From the slope of this line we can evaluate an equivalent lattice contraction β' about four times lower than the original one. Since the stress is released about two times through dislocation generation, there is no reason to believe that lattice contraction will be reduced four times. A similar, two-times reduction in the overall lattice contraction coefficient should be a sensible supposition. This means a return path denoted in Fig. 5 with e, which does not contain the origin. If this is true, to completely release the residual tensile stress, removal of only a fraction of boron atoms is necessary. Further decrease of boron concentration is equivalent to doping with silicon a lattice that is now slightly smaller than the silicon lattice. Silicon atoms produce a compressive stress. This phenomenon can explain why cantilevers that were bended upward before the thermal annealing became strongly bended downward after thermal annealing. During oxidation/drive-in, the profile developed in the depth of the layer supposes a region where the concentration of boron is always increasing, compared with the as-diffused samples and a region where the concentration is always decreasing as the treatment proceeds (Fig. 6). In the region with increasing boron concentration the stress will be always tensile, while in the region where the concentration decreases the compressive stress will develop.

Raman spectra measured on both sides of etched microstructures are strongly related to boron concentrations in the near-surface region. Linewidth variations from $12\ cm^{-1}$ to $20\ cm^{-1}$ are associated with boron levels from

Table 2 Features of Raman spectra in p^+ cantilevers and bridges.

Structure side	$\delta_{bridge} - \delta_{cant}$	$FWHM_{bridge} - FWHM_{cant}$
top	1.5−1=0.5 cm^{-1}	15.43−13.69=1.74 cm^{-1}
back	1−0 5=0 5 cm^{-1}	14.52−12 86=1.66 cm^{-1}

5×10^{19} cm^{-3} to 1.5×10^{20} cm^{-3}. Given the relatively constant level of boron at the etched interface, monitoring the top surface of the wafer during the fabrication process allows the prediction of the behavior of the final structure. Such measurements have the advantages of high spatial resolution, compatibility with a mask layer of silicon dioxide, and ease of use. To separate the effects of boron concentration from the effects of stress and crystalline disorder, Raman measurements on cantilevers and bridges were performed and the results are presented in Table 2. The difference is remarkably large, but some nonuniformities in our diffusion process prevent us from putting some definite conclusions to this issue.

2.1.5 *Stress anisotropy in p + silicon*

The mechanical condition (flat or buckled) and the resonance frequency of bridges were used to evaluate the residual stress in $p+$ layers. Arrays of bridges and diaphragms with lengths from 1 to 6 mm and widths ranging from 200 microns to 6 mm were fabricated in the ⟨110⟩ and ⟨100⟩ direction of (100) wafers.

On the as-diffused samples all the bridges and diaphragms, of all lengths and widths, were always flat and under tensile stress. The resonance tests gave a residual tensile stress of about 20 MPa for such bridges.

On the oxidized samples, however, a mixed behavior was found. All the narrow bridges (width up to 700 microns) were flat, irrespective of their length (even those of 6 mm length) and with the same tensile stress of 20 MPa resulting from resonance frequency measurements. On the other hand, wider bridges (length 6 mm, width over 1 mm) on the same wafer and the diaphragms were found to be buckled, indicative of a compressive stress exceeding the critical stress. The calculated critical buckling stress for those bridges is − 0.24 MPa.

We suggest that a stress anisotropy in the $p+$ layer might be responsible for this behavior. Preliminary measurements of rocking curves obtained from x-ray diffraction measurements supported our supposition. More experimental work has to be done, though, in order to confirm the hypothesis and to give a quantitative description of the phenomenon. We can speculate on the fact that a tilt in the lattice subsequent to an oxidation/annealing process could introduce unwanted mechanical unbalances in the fabricated structures, resulting in reduced quality factors, increased mechanical coupling, and finally noise.

2.2 *Young's Modulus of p + Silicon*

Young's modulus of $p+$ silicon was evaluated by fitting the measured value of the resonance frequency of $p+$ silicon cantilevers to the frequencies simulated with ANSYS. (The curvature associated with the diffusion profile was considered.) Beams with lengths between 1500 and 2000 μm, with a width of 200 μm and thickness around 4 μm, were fabricated. To precisely evaluate Young's modulus from the resonance frequency of a cantilever beam, the geometrical dimensions of the beam have to be precisely known. While the lateral dimensions can be easily obtained from a calibrated $x-y$ stage, obtaining the thickness of the beams is more difficult. The method used was to first measure the resonance frequency and then to bond the beams to a glass plate followed by the thickness measurements using a surface profiler. The values obtained for the Young's modulus are given in Table 3. The average value obtained for Young's modulus of $p+$ silicon is 1.33×10^{11} Pa. The errors are + 12.78% to − 10%, smaller than the previously reported ones of about 20%. The Young's modulus of the low-doped silicon for the same crystallographic direction is 1.7×10^{11} Pa. The elastic constant was reduced by the plastic deformations produced and/or the high level of impurities.

Table 3 Young's modulus of $p+$ silicon.

Structure code	Length (μm)	Thickness (μm)	f_{rez} (Hz)	E (10^{11}Pa)
7-1	2057	4.2	1264 062	1.44
7-2	2056	4.2	1266.994	1.45
7-3	1556	4.0	1917.868	1.53
7-5	1486	3.9	2129.321	1.29
7-6	1485	3 9	2082 66	1.23
7-7	1887	3.9	1301.129	1.25
7-8	1888	4.0	1343 180	1.27
9-3	1545	3 9	2010.323	1.35
9-4	1551	4.0	1932 181	1.20

2.3 *Intrinsic Losses of p + Silicon*

Monocrystalline silicon is considered an almost ideal material for resonators, because the monocrystal is supposed to have minimal internal losses. To evaluate the impact of the high boron concentration on the internal losses, similar cantilevers were realized in $p+$ silicon and in low-doped silicon.[20] To control the thickness of the low-doped resonators to the same value as the thickness of the $p+$ resonators, the *in situ* optical monitoring method was used.[15] The quality factors measured for cantilevers with the resonance frequency of about 10 kHz at a vacuum level of 2.5 $\times10^{-6}$ Torr are given in Table 4. The intrinsic losses are higher in the highly doped silicon.

A variation in the value of the Q factor was observed for the $p+$ silicon structures, related to the density of lattice

Table 4 Internal losses of $p+$ silicon.

Structure type	f_{rez} (kHz)	Q	Internal losses
Si Cantilever	9 834 kHz	420,000	1.2×10^{-6}
$p+$ Si Cantilever	10.10 kHz	250,000	2×10^{-6}

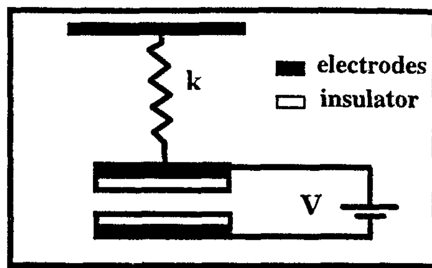

Fig. 7 Schematic structure of a touch-mode electrostatic actuator.

defects. The lattice defects appearing in the $p+$ layers are the line dislocations and the stacking faults. The structures with a lower density of dislocations and stacking faults showed a Q factor twice the value found in similar structures having higher densities of lattice defects.

2.4 *Thermal Expansion of p + Silicon*

The temperature behavior of $p+$ silicon cantilevers and bridges was monitored and it resulted in a temperature coefficient of the resonance frequency of a cantilever of about -5.76 ppm/°C (vs. -32 ppm/°C for low-doped silicon) while the temperature coefficient of the resonance frequency of a $p+$ bridge was about $+200$ ppm/°C. This means that the thermal expansion coefficient of $p+$ silicon is smaller than that of the low-doped silicon and could also be process dependent. The difference in the thermal expansion of the $p+$ silicon and of the low-doped silicon has to be considered when producing stress-sensitive $p+$ resonators anchored in a low-doped silicon wafer. Such resonators will have an important temperature sensitivity compared with a low-doped silicon structure.

3 Touch-Mode Electrostatic Microactuators

The basic structure of a touch-mode electrostatic actuator is that of a condenser that has at least one movable electrode (Fig. 7). To prevent an electrical short, the electrodes are covered with an insulator.

While from the electrical point of view the electrode has as its single relevant characteristic the resistivity, which is not critical for the actuation process, introducing an insulating layer brings a wealth of parameters and phenomena into the picture.

The most used formula for the electrostatic force is relating it to the voltage applied between two electrodes:

$$F_{el}=\frac{\epsilon A}{2d^2}V^2, \tag{2}$$

where ϵ is the dielectric constant of the medium in the gap, A is the area of the two electrodes, d is the distance between the electrodes, and V is the applied voltage. However, an applied voltage does not always result in the desired electrostatic force. A better description of electrostatic force generation is given by the formula

$$F_{el}=\tfrac{1}{2}QE_o, \tag{3}$$

which states that in order to generate an electrostatic force, a charge Q and an electrostatic field E_o are required.

The charge Q needed in the electrostatic actuation can be generated by a voltage supply. Material properties and the interactions at the various interfaces of the structure will, however, decide the final charge and field distribution. Such effects can sometimes jeopardize the actuation process.

An insulator is characterized by

1. the dielectric strength
2. the relative dielectric constant
3. the density of interface states (ideally zero)
4. the density of permanently or temporarily chargeable traps (ideally zero)
5. the surface conductivity (ideally zero).

The insulators used in silicon technology are silicon oxides and silicon nitrides. Table 5 gives some relevant parameters for such dielectrics[22–25] and Fig. 8 shows the C-V characteristics measured on such layers. If not speci-

Table 5 Properties of some silicon-based dielectrics.

Property\Dielectric	Thermal SiO_2	PECVD SiO_2	LPCVD Si_3N_4	Sputtered SiN	PECVD SiN
Dep. Temperature	800 1200 °C	200 °C	700 800 °C	200 °C	300 °C
Stress (MPa)	−200 −400	−300 . +300	+1000.. +1800	−300.. −1600	−100 −800
Step Coverage	-	Good	Fair	Poor	Conformal
ϵ_ρ	3.9	3 9	6-7	6-12	6-9
Diel Strength (V/cm)	5. 10×10^6	8×10^6	10^7	10^6 6×10^6	6×10^6
Bulk resistivity (ohm-cm)	10^{14} 10^{16}		$10^{15}-10^{17}$	$5\times10^{12}-6\times10^{15}$	10^{15}
C-V Hysteresis	0 1 V	7V	3.5V	?	40V
$\Delta C/\Delta V$ Stretching	1 V^{-1}	1/7 5 V^{-1}	1/2.66 V^{-1}	1/208 V^{-1}	1/3 V^{-1}
Water permeability	high		zero		low

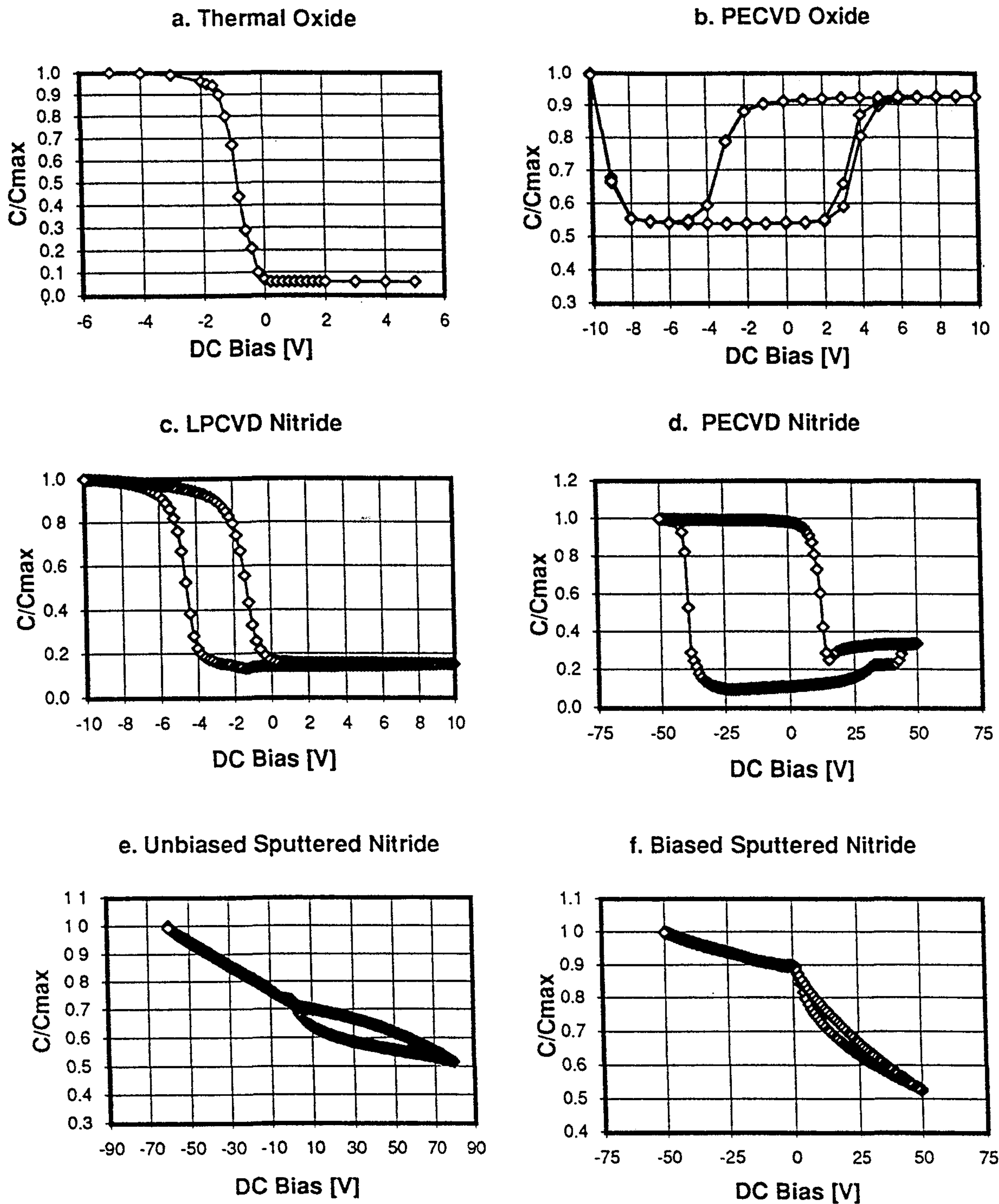

Fig. 8 High-frequency *C–V* characteristics of some dielectrics used in silicon technology.

fied, the thickness of the dielectric in the test capacitors is 1000 Å. In the last line of Table 5, the behavior toward water was mentioned, since in many micromachined devices, the dielectric could be exposed to humid air. Surface conductivity of all dielectrics can vary with orders of magnitude depending on the environmental humidity.

The very high temperature required by the oxidation of silicon prevents its use in later stages of the fabrication process, when some temperature-sensitive layers (e.g., metals) have already been introduced in the structure. Sputter deposited (SD) and plasma-enhanced CVD (PECVD) dielectrics are interesting alternatives. In both processes, the temperature of the substrate during deposition is below 400 °C, allowing metals to be included in the structures. However, the low-temperature materials are known as poor dielectrics. It was considered that, while not acceptable in

the gate of MOS devices (except for some layers used in memories), such dielectrics could still be used in the electrostatic actuators, where just an insulator is needed. It turns out that this is not the case.

High-frequency C-V curves (1 MHz) were measured for thermal oxide (1000 Å), Fig. 8(a), PECVD oxide (500 Å), Fig. 8(b), LPCVD nitride (1000 Å), Fig. 8(c), PECVD nitride (1000 Å), Fig. 8(d), unbiased sputtered nitride (1000 Å), Fig. 8(d), and biased sputtered nitride (1000 Å), Fig. 8(e). Except for the thermal oxide, the characteristics show hysteresis, stretch-out, and drift, indicative of charge injection and retention in dielectric traps.

The effects of surface charge, charge injection, and charge retention on the touch-mode electrostatic actuators are:

1. wide variations in the actuation voltages
2. environmental dependence of the actuation voltage
3. electrostatically induced stiction.

None can be accepted. In most cases, the electrostatic actuators are working in conditions significantly harder than the MOS devices. The dielectric is exposed to (humid) air, the fields are high, the charge distribution is changing as a result of actuator movement, and important modification can occur at the interface as the two insulated electrodes come into contact. Any conductive layer on the surface of the dielectric will produce zero field at the interface and the actuation will be jeopardized. By no means can the dielectric used in electrostatic actuators be tolerant to electrical flaws.

4 Conclusions

To get control over the third dimension of micromachined single-crystal silicon structures, a simple process step can be used: diffusion of boron at concentrations over $6\times10^{19}\ \mathrm{cm}^{-3}$. This step produces, however, important changes in the electrical, optical, and mechanical characteristics of the single crystal silicon. The material is highly degenerated (Fermi level deep inside the valence band), the absorption in IR highly increased, the modulus of elasticity is reduced, the intrinsic losses are increased, the layer is under a critically changing stress, the thermal expansion coefficient is modified, resulting in increased temperature effects, and new anisotropies are introduced in the materials. Most of these unwanted side effects of the heavy boron doping are produced by the plastic deformation of the lattice. To keep them under control, boron doping at levels between the etch-stop level ($6\times10^{19}\ \mathrm{cm}^{-3}$) and the critical level producing plastic deformations ($1.1\times10^{20}\ \mathrm{cm}^{-3}$) should be performed. Such a concentration control could be achieved by ion implantation. The electro-optical effects cannot be avoided, and the better approach is to use them.

To arrive at such detailed findings, SIMS, MRS, Fourier transform infrared (FTIR) spectrometry, calibrated microscopy, resonance methods, and x-ray diffraction together with ANSYS simulations were used, showing the complexity of the characterization work to be done in MOEMS devices.

Concerning the electrostatic actuators, the re-evaluation of the low-temperature dielectrics (sputtered nitrides and the PECVD oxides and nitrides) showed that the large amount of injected and trapped charge in such dielectrics is incompatible with the actuation process. It can introduce a time dependence of the actuation voltage, electrostatically induced stiction, and finally complete failure of the actuation process. In addition to the dielectric/electrode interface, the exposed surface of the dielectric can introduce a new set of problems that have to be addressed.

In conclusion, it can be said that MOEMS are highly demanding in terms of materials needs since they have to face the real world, performing, at the same time, in the optical, electronic, electrical, and mechanical domains. The precise limits of process variation that allow increased manufacturability without compromising the mechanical and opto-electrical characteristics has to be found and the process finely tuned. To do that, extensive and refined characterization must still be done.

Acknowledgments

Part of the research reported in this paper was performed at Tohoku University, Japan, in the laboratory of Professor Esashi, who is highly acknowledged.

Dawn Murphy, Steve Johnston, and Eugen Cabuz from Honeywell Technology Center are highly acknowledged for the fabrication and evaluation of the numerous test structures.

References

1. D W. Burns, W R Herb, J. D. Zook, and M. L Wilson, "Optically driven resonant microbeam temperature sensors for fiber optic networks," *Technical Digest of the Solid State Sensor and Actuator Workshop*, Hilton Head, SC, June 3–6, 1996, pp. 294–299 (1996)
2. J. A. Walker, K W. Gossen, S C. Arney, N. J. Frigo, and P. P. Iannone, "A silicon optical modulator with 5 MHz operation for fiber-in-the-loop applications," *Transducers '95*, Stockholm, Sweden, June 1995, pp 285–288 (1995).
3. J. K Robertson and K D Wise, "An electrostatically-actuated microvalve for semiconductor gas flow control," *Technical Digest of the Solid State Sensor and Actuator Workshop*, Hilton Head, SC, June 3–6, 1996, pp 148–151 (1996).
4. G. Kaminsky, "Noncontaminating si-based shadow masks for MBE," *J. Vac Sci Technol* **B3**, 741–742 (1985)
5. J Ji and K. D. Wise, "An implantable CMOS analog signal processor for multiplexed microelectrode recording arrays," *Tech Digest. IEEE Solid-State Sensors and Actuators Workshop*, pp. 107–110, Hilton Head, SC (1990).
6. Y Gianchandani and K. Najafi, "A bulk silicon dissolved wafer process for microelectro-mechanical systems," *Tech Dig IEDM*, pp. 29.5 1–29 5 4, Washington, DC (1991).
7. M A Huff, S. D. Senturia, and R T Howe, "A thermally isolated microstructure suitable for gas sensing applications," *Tech. Digest IEEE Solid-State Sensor and Actuator Workshop*, pp 47–50, Hilton Head, SC (1988)
8. K. Ikeda, H Kuwayama, T. Kobayashi, T. Watanabe, T Nishikawa, and T. Yoshida, "Silicon pressure sensor with resonant strain gauge built into diaphragm," *Tech Digest 7th Sensor Symp.*, pp. 55–58, Tokyo, Japan (1988)
9. C Cabuz, K Fukatsu, H Hashimoto, S Shoji, T. Kurabayashi, K. Minami, and M Esashi, "Fine frequency tuning in resonant sensors," *Proc IEEE Micro Electro Mechanical Systems, MEMS'94*, pp. 245–250, Oiso, Japan (1994)
10. K. Suzuki, "Study on silicon capacitive microsensors and electrostatic microactuators: toward a micro electro mechanical system (MEMS)," PhD dissertation, Tohoku University (1993)
11. C Cabuz, S Shoji, K Fukatsu, E Cabuz, K Minami, and M Esashi, "Highly sensitive resonant infrared sensor," *Tech Digest Int Conf Solid-State Sensors and Actuators, Transducers '93*, pp 694–697, Yokohama, Japan (1993)
12. B Kloeck, "A novel four electrode electrochemical etch-stop method for silicon membrane formation," *Tech Digest Int Conf Solid-State Sensors and Actuators, Transducers '87*, pp 116–119, Tokyo, Japan (1987)
13. K. J Ma and K Najafi, "A new capacitive electro-chemical etch-stop technique," *Proc IEEE Micro Electro Mechanical Systems, MEMS'94*, pp 158–163, Oiso, Japan (1994)

14. E Peeters, D Lapadatu, W Sansen, and B Puers, "PHET-an electrodeless photovoltaic electrochemical etchstop technique," *Tech Dig Int Conf Solid-State Sensors and Actuators, Transducers '93*, pp 254–257, Yokohama, Japan (1993).
15. K Minami, H. Tosaka, and M. Esashi, "Optical *in-situ* monitoring of silicon diaphragm thickness during wet etching," *Proc IEEE Micro Electro Mechanical Systems, MEMS'94*, pp 217–222, Oiso, Japan (1994).
16. J. Bernstein, S Cho, A T King, A. Kourepenis, P Maciel, and M. Weinberg, "A micromachined comb-drive tuning fork rate gyroscope," *Proc IEEE Micro Electro Mechanical Systems, MEMS'93*, pp 143–148, Fort Lauderdale, FL (1993).
17. J Herzog, L. Csepregy, and H Seidel, "X-ray investigation of boron- and germanium-doped silicon epitaxial layers," *J Electrochem Soc* **131**, 2969–2974 (1984)
18. C Cabuz, K. Fukatsu, T. Kurabayashi, K. Minami, and M. Esashi, "Microphysical investigations on mechanical structures realized in $p+$ silicon," *J-MEMS* 4(3), 109–118 (1995).
19. C. Cabuz, "Silicon micromachined resonators for sensor applications," PhD dissertation, Tohoku University, Sendai, Japan (June 1994)
20. K Fukatsu, C Cabuz, and M Esashi, "Internal friction of $p+$ silicon," Japan Soc. of Next Generation Sensor Technology, Micromachining Technical Report MM-94-95, pp 33–38, Tokyo (1994)
21. F H Horn, "Densitometric and electrical investigation of boron in silicon," *Phys Rev* **97**, 1521–1525 (1955)
22. E H Nicollian and J. R Brews, MOS *(Metal Oxide Semiconductor) Physics and Technology*, John Wiley & Sons, New York (1982).
23. S. M Sze, *Physics of Semiconductor Devices*, John Wiley & Sons, New York (1981).
24. J T Milek, *Handbook of Electronic Materials, Vol 3, Silicon Nitride for Microelectronic Applications*, Plenum Press, New York (1971).
25. S Wolf and R. N. Tauber, *Silicon Processing for the VLSI Era*, Vol. 1, Lattice Press (1986).

Cleopatra Cabuz received the MS degree in electronics and telecommunications in 1979 from the Politehnica University of Bucharest (PUB), Romania, and the PhD degree in engineering in 1994 from Tohoku University, Sendai, Japan. Between 1984 and 1995 she held several research and teaching positions at PUB Between 1991 and 1994 she spent two years as a Visiting Researcher and Research Associate at Tohoku University She is currently with Honeywell Technology Center, Minneapolis. Her current research interests include material study and characterization, resonant sensors, low power actuators, and inertial sensors.